Physica C 470 (2010) 61–67

Contents lists available at ScienceDirect

Physica C

journal homepage: www.elsevier.com/locate/physc

Magnetoresistance hysteresis of bulk textured $Bi_{1.8}Pb_{0.3}Sr_{1.9}Ca_2Cu_3O_x$ + Ag ceramics and its anisotropy

D.A. Balaev [a,b], S.I. Popkov [a], S.V. Semenov [a,b], A.A. Bykov [a], K.A. Shaykhutdinov [a,b], D.M. Gokhfeld [a,*], M.I. Petrov [a]

[a] L.V. Kirensky Institute of Physics, Krasnoyarsk 660036, Russia
[b] Siberian Federal University, Krasnoyarsk 660041, Russia

ARTICLE INFO

Article history:
Received 9 June 2009
Received in revised form 4 September 2009
Accepted 5 October 2009
Available online 8 October 2009

Keywords:
Magnetoresistance
Anisotropy
Scaling
Magnetization
Bi2223
BSCCO

ABSTRACT

Magnetoresistance of bulk textured $Bi_{1.8}Pb_{0.3}Sr_{1.9}Ca_2Cu_3O_x$ + Ag ceramics has been studied in the magnetic fields applied parallel and perpendicular to *a–b* planes of Bi2223 crystallites. Besides well known anisotropy of magnetoresistance of textured superconductors ($R_{H\,||\,c} > R_{H\,||\,a-b}$), anisotropic hysteresis of $R(H)$ dependences was investigated. Parameters characterizing hysteretic $R(H)$ curves differ for the cases $\boldsymbol{H}\,||\,c$ and $\boldsymbol{H}\,||\,a$–*b*. This behavior is explained within the model of a granular superconductor where the total magnetic induction in the intercrystallite boundaries is superposition of the external field and the magnetic field induced by dipole magnetic moments of neighbor crystallites.

1. Introduction

Hysteretic behavior of magnetoresistance $R(H)$ and critical current $I_c(H)$ of granular high-T_c superconductors (HTSCs) in external magnetic field H has been revealed soon after discovery of HTSCs [1,2]. Systematic experiments focused on understanding of mechanisms responsible for the hysteretic magnetoresistance (HMR) have appeared during past few years [3–13]. A granular structure of HTSCs is found to be responsible for HMR [10]. The superposition of external field and local fields induced by magnetic dipole moments of neighbor superconducting crystallites in the intercrystallite boundaries causes the specific character of HMR. Detail study of HMR of the weakly coupled composite system Y–Ba–Cu–O + CuO [10] and 'pure' granular Y–Ba–Cu–O, Bi–Ca–Sr–Cu–O, and La–Sr–Cu–O [13] at various transport currents has shown that $R(H)$ dependences may be characterized by the field width of hysteresis ΔH, the current-independent parameter depending on the crystallite pinning.

The textured Bi-based HTSC system is rather interesting object for studying of HMR because the textured ceramics demonstrate the anisotropy of magnetization with respect to the orientation of external field and crystallographic axes of superconducting crystallites. Therefore, it is possible to observe the correlation between hysteretic properties of magnetization and HMR. Previous studies of transport properties of Bi-based textured samples focused on the dependence of critical current and magnetoresistance on the angle between $\boldsymbol{H}$ and *c*-axis [14–19]. In this paper we have studied HMR of textured Bi2223 + Ag ceramics for orientations $\boldsymbol{H}\,||\,a$–*b* and $\boldsymbol{H}\,||\,c$.

2. Experimental details

The preparation of bulk textured 70 vol.% $Bi_{1.8}Pb_{0.3}Sr_{1.9}Ca_2Cu_3O_x$ + 30 vol.% Ag ceramic samples used in these experiments[1] is described in [20]. In these textured ceramics the plate-like Bi2223 crystallites have thickness 1–2 μm along *c*-axis and average linear dimensions ~20 × 20 μm in *a–b* plane. The critical temperature T_c determined from the magnetic measurements is 108 K. The critical

* Corresponding author. Address: L.V. Kirensky Institute of Physics SD RAS, High Magnetic Fields Lab, Akademgorodok, 50/38, 660036 Krasnoyarsk, Russia. Tel.: +7 391 2494838.
E-mail addresses: smp@iph.krasn.ru, gokhfeld@yandex.ru (D.M. Gokhfeld).

0921-4534/$ - see front matter © 2009 Elsevier B.V. All rights reserved.
doi:10.1016/j.physc.2009.10.007

[1] Similar data have been obtained for textured $Bi_{1.8}Pb_{0.3}Sr_{1.9}Ca_2Cu_3O_x$ without Ag additions (not presented here).

current density j_c is ≈ 220 A/cm^2 at T = 77.4 K. The value of resistivity just above resistive transition (113 K) is ≈ 0.4 mΩ cm [20]. The maximal magnitude of magnetoresistance at T = 77.4 K obtained at transport current I = 1000 mA and external field H = 12 kOe is about 10% of resistance of this sample above resistive transition (113 K).

The magnetoresistance $R(H) = U(H)/I$ (where U is the voltage drop) was measured by the standard four-probe technique. The samples have dimensions 0.5 × 0.5 × 10 mm^3. The constant transport current I up to 1000 mA was applied along the a–b planes of Bi2223 crystallites (along the largest dimension of sample). The external magnetic filed $\boldsymbol{H}$ was applied normal or parallel to a–b planes of crystallites and was always perpendicular to transport current direction, see Fig. 1. Electrical contacts were made using the epoxy Ag paste. The sample was cooled in zero magnetic field. During $R(H)$ measurements the sample was immersed in the liquid nitrogen bath so self-heating of the sample was negligible.

Magnetic measurements have been performed using the vibration sample magnetometer. The sample of cubic form 0.5 × 0.5 × 0.5 mm^3 was cut from the same sample that was before used for transport measurements.

3. Results and discussion

3.1. Anisotropy of magnetic and transport properties

3.1.1. Anisotropy of magnetic hysteretic loops

The textured sample under study demonstrates an anisotropy of magnetization $M(H)$ with respect to the orientation of $\boldsymbol{H}$ and a–b planes of the crystallites. The diamagnetic response for $\boldsymbol{H} \parallel a$–$b$ is smaller in 1.7 times than for $\boldsymbol{H} \parallel c$ (see Figs. 2 and 3a). This anisotropy originates from the intrinsic anisotropy of Bi2223 crystallites. The critical state model [21] is usually used for extraction of a field dependence of the crystallite critical current density: $j_c(H) \sim \Delta M(H)/d$, where $\Delta M(H) = |M(H_\uparrow) - M(H_\downarrow)|$, at $H = H_\downarrow = H_\uparrow$, and d is the size of crystallites. Hereafter we denote $H = H_\uparrow$ and

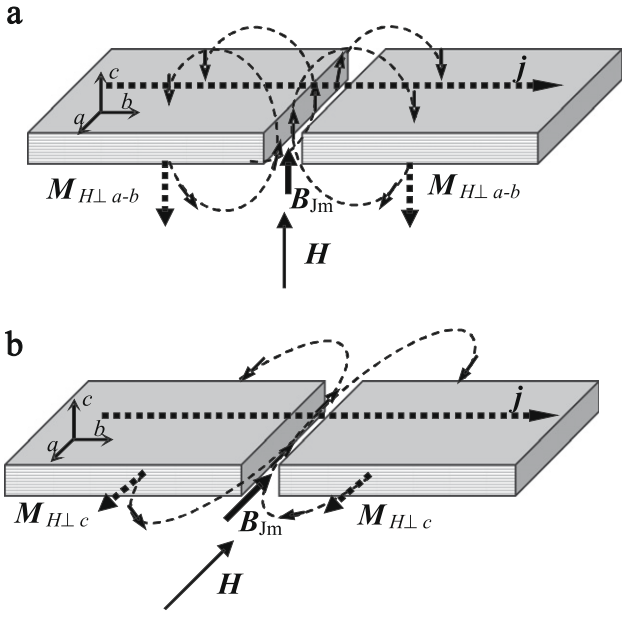

Fig. 1. Schematic representation of fields and transport current in a granular superconductor. Total magnetic induction B_{Jm} in the intercrystallite separation. (a) External field $\boldsymbol{H}$ applied parallel to c-axis of Bi2223 crystallites. (b) External field $\boldsymbol{H}$ applied parallel to a–b-planes of Bi2223 crystallites. M is magnetic moment of Bi2223 crystallite when H is increased (magnetization is negative). Dashed lines are lines of magnetic induction from the screening currents in crystallites. Dotted line is the direction of transport current I.

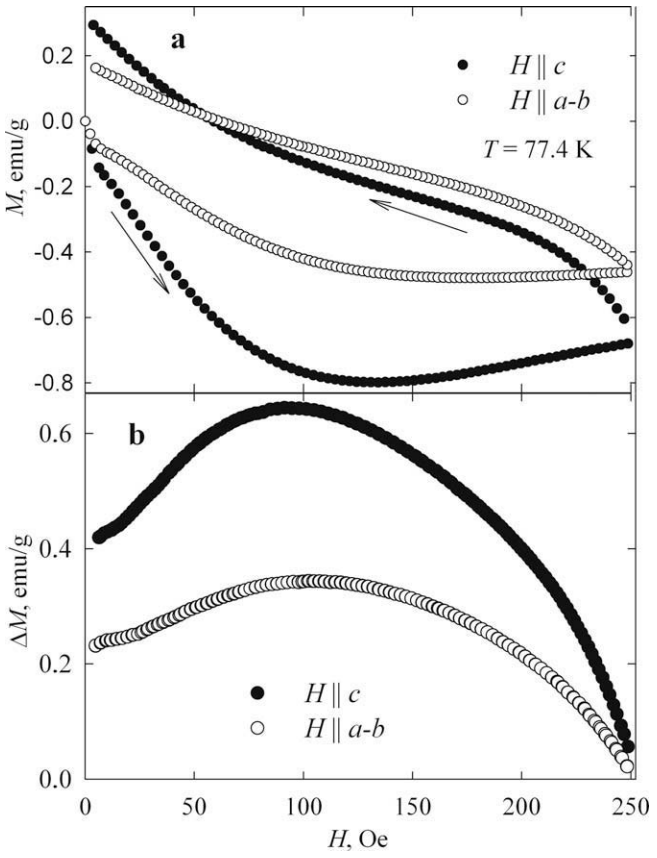

Fig. 2. Magnetization of textured ceramic for $\boldsymbol{H} \parallel c$ and $\boldsymbol{H} \parallel a$–$b$ at T = 77.4 K (H_{max} = 250 Oe). (a) Hysteretic magnetization $M(H)$. (b) The difference $\Delta M(H) = M(H_\uparrow) - M(H_\downarrow)$. Arrows indicate the direction of scanning of external field.

$H = H_\downarrow$ for increasing or decreasing external field correspondingly. At high temperatures, however, an extraction of correct dependence of $j_c(H)$ from $\Delta M(H)$ is complicated because influence of the vortex pinning becomes comparable with the geometric barrier or Bean-Livingston barrier [22,23]. Nevertheless, the approximate proportionality of ΔM to the crystallite j_c should holds. So we assume that the $\Delta M(H)$ dependences behave similarly to $j_c(H)$ ones, i.e. $\Delta M_{H \parallel c}(H)$ is proportional to the crystallite critical current density in the a–b plane, $\Delta M_{H \parallel c}(H) \sim j_c^{a-b}(H)$, and $\Delta M_{H \parallel a-b}(H)$ is proportional to the critical current density along the c-axis, $\Delta M_{H \parallel a-b}(H) \sim j_c^{c}(H)$. It is seen from Figs. 2 and 3b that $\Delta M_{H \parallel c}(H) > \Delta M_{H \parallel a-b}(H)$ in the low-field range ($H \leqslant 400$ Oe), while $\Delta M_{H \parallel c}(H) < \Delta M_{H \parallel a-b}(H)$ in the range of intermediate fields $H \geqslant 400$ Oe. This behavior reflects the well known feature of Bi2223 system: the $j_c^{a-b}(H)$ dependence decreases faster than $j_c^{c}(H)$ [19,23,24]. Fig. 4 shows the $M(H)$ dependences in the range 0–5 kOe (external field was cycled up to 20 kOe). The irreversibility field, at which the forward and the reverse branches of $M(H)$ begin to coincide, is estimated to be 1800 ± 100 Oe for $\boldsymbol{H} \parallel c$ and 3800 ± 200 Oe for $\boldsymbol{H} \parallel a$–$b$. This is in accordance with the data obtained for Bi2223 system by other groups from magnetic [23–25] and transport [18] measurements. The behavior of $M(H)$ and $\Delta M(H)$ dependences is crucial for understanding of hysteretic properties of $R(H)$ curves (see below).

3.1.2. The contributions from intercrystallite boundaries and Bi2223 crystallites to the magnetoresistance

Fig. 5 shows magnetoresistance curves measured at transport currents 100–1000 mA in both $\boldsymbol{H} \parallel a$–$b$ and $\boldsymbol{H} \parallel c$ directions. The anisotropy of magnetoresistance with respect to orientation of H and crystallographic axes of Bi2223 crystallites is clearly seen:

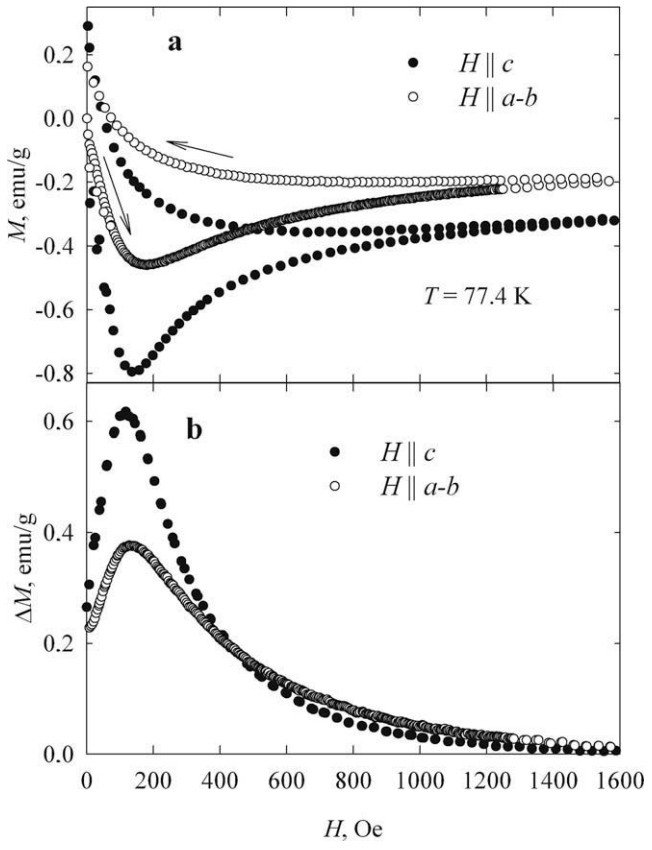

Fig. 3. Magnetization of textured ceramic for $\boldsymbol{H} \parallel c$ and $\boldsymbol{H} \parallel a$–$b$ at $T = 77.4$ K ($H_{max} = 1600$ Oe). (a) Hysteretic magnetization $M(H)$. (b) The difference $\Delta M(H) = M(H_1) - M(H_1)$. Arrows indicate the direction of scanning of external field.

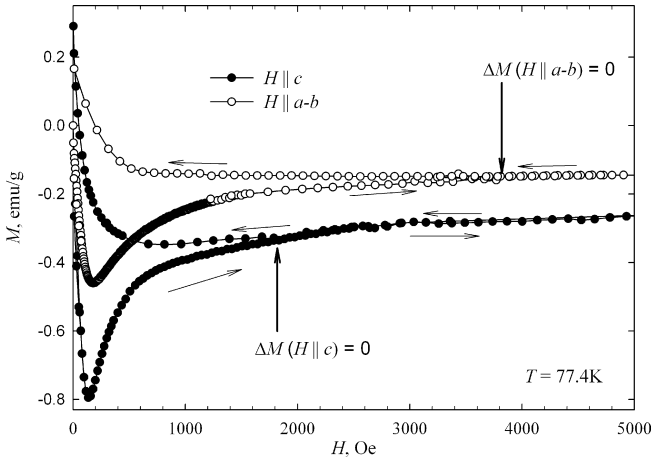

Fig. 4. Hysteretic magnetization $M(H)$ of textured ceramic for $\boldsymbol{H} \parallel c$ and $\boldsymbol{H} \parallel a$–$b$ at $T = 77.4$ K ($H_{max} = 20$ kOe). Thin arrows indicate direction of scanning of external field. Bold arrows mark the field of irreversibility.

$R_{H \parallel c}$ is larger than $R_{H \parallel a-b}$. Similar behavior have been reported for textured $(Bi,Pb)_2Sr_2Ca_2Cu_3O_y$ silver-clad tape [14]. Additionally the $R(H)$ curves in Fig. 5 have a peculiarity which was not pointed out in cited work [14]. At high transport currents ($I > 200$ mA) the magnetoresistance firstly saturates at $H \sim 1$ kOe and then the $R(H)$ dependences change the curvature (about $H \sim 2$ kOe for $\boldsymbol{H} \parallel c$ and $H \sim 4$ kOe for $\boldsymbol{H} \parallel a$–$b$) following by further increase of resistance. Such a behavior is evidently related to contribution of the intercrystallite boundaries to magnetoresistance. Namely the dissipation begins in the boundaries between Bi2223 crystallites at external magnetic fields less than several kOe at sufficiently high temperatures ($T > 50$ K). The change of curvature of the $R(H)$ dependences corresponds to the onset of dissipation within Bi2223 crystallites (the similar effect was observed in YBCO systems [6]). Really, according to magnetic measurements, see Section 3.1.1, the crystallite j_c becomes vanishingly small at $H > 2$ kOe for $\boldsymbol{H} \parallel c$ and at $H > 4$ kOe for $\boldsymbol{H} \parallel a$–$b$. So, the magnetoresistance is contributed from two subsystems: intercrystallite boundaries and Bi2223 crystallites. At high transport current the former contribution is dominating in the range $H < 2$ kOe and the latter is dominating in the range $H > 2$ kOe. At the low transport current both contributions seem to take place at $H > 2$ kOe.

3.1.3. Scaling of magnetoresistance curves

The effective-mass model for anisotropic superconductor [26,27] predicts the scaling of $R(H)$ dependences for different angles θ between $\boldsymbol{H}$ and c-axis of crystallites. All the $R(H)$ dependences at a certain temperature should coincide if they be replotted as $R(H^*)$, where the effective field $H^* = H\sqrt{\gamma^{-2}\sin^2\theta + \cos^2\theta}$, γ is the anisotropy parameter, and θ is the angle between $\boldsymbol{H}$ and c-axis. According to this scaling approach $R_{H \parallel c}(H) = R_{H \parallel a-b}(\gamma H)$. In Fig. 6 the magnetoresistance curves are replotted as $R_{H \parallel c}(H)$ and $R_{H \parallel a-b}(\gamma H)$ dependences. These curves coincide satisfactorily for $\gamma = 1.95$. The coincidence in Fig. 6 is best for high magnetic field range where the dissipation in crystallites contributes mainly to $R(H)$. In the range of low and intermediate magnetic fields the magnetoresistance of sample is determined by the intercrystallite boundaries and parameter γ has probably the different nature.

The estimated γ is similar to the results for textured Bi2223 samples with the similar geometry of experiments [14,15,17,28]. This value of γ is much smaller than the anisotropy parameter j_c^{a-b}/j_c^c for a single crystal of Bi2223 which known to be 50–100. The misalignment of the crystallites is partially responsible for this difference. However the commonly observed decrease of the anisotropy of the textured HTSCs in 20–50 times in comparison with single crystals [14,15,17,28] is unclear and required further investigations.

3.2. Anisotropy of hysteresis of magnetoresistance

3.2.1. Correlation of hysteresis of magnetoresistance and magnetization

Fig. 7 shows portions of magnetoresistance curves at $I = 400$ mA in the field range up to 5 kOe. In these measurements the external field was cycled up to various maximal values H_{max} and after every measurement the sample was heated up to $T > T_c$. It is seen that the $R(H)$ dependences are hysteretic in the range $H \leqslant 1750 \pm 150$ Oe for $\boldsymbol{H} \parallel c$ and $H \leqslant 3600 \pm 200$ Oe for $\boldsymbol{H} \parallel a$–$b$. It correlates with the behavior of $M(H)$, see Fig. 4 and Section 3.1.1. We did not observe a visible effect of variation of transport current in the range where the hysteresis of $R(H)$ exists. So, one can conclude that the $R(H)$ dependences are hysteretic in the same field range as the $M(H)$ ones.

Figs. 8 and 9a show typical HMR curves in both $\boldsymbol{H} \parallel a$–$b$ and $\boldsymbol{H} \parallel c$ directions measured when the field was cycled up to 250 Oe and 1600 Oe correspondingly (similarly to the $M(H)$ curves presented in Figs. 2 and 3a).

Let us consider the effect of magnetic moments of crystallites on the magnetic induction in the intercrystallite media in the field range $H < 2$ kOe where the magnetoresistance is caused by dissipation in the intercrystallite boundaries. When H is larger than the first critical field of the intercrystallite media[2] the total magnetic

[2] Initial branch of $M(H)$ curves (Fig. 2a) exhibits a kink at $H \sim 6$ Oe. In [29] the similar kink observed at nearly the same external field at $T = 77$ K was interpreted as the first penetration field in the intercrystallite (Josephson) media.

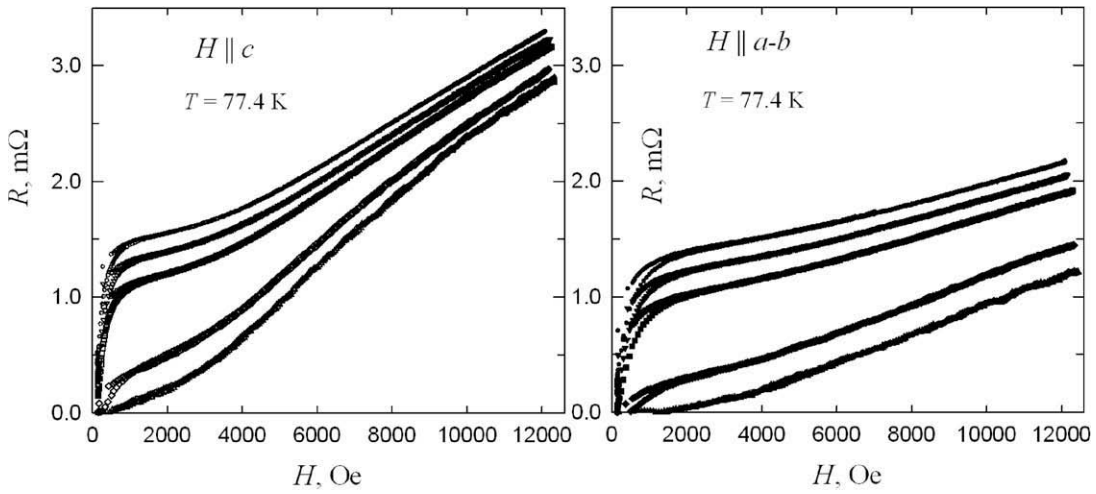

Fig. 5. Magnetoresistance $R(H)$ of textured ceramic for $\boldsymbol{H} \parallel c$ and $\boldsymbol{H} \parallel a$–$b$ at $T = 77.4$ K at transport currents 100, 200, 600, 800, and 1000 mA (from bottom to top).

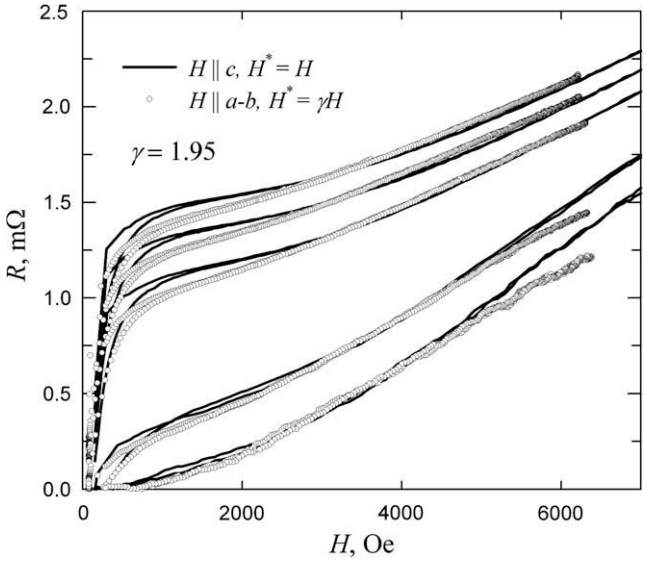

Fig. 6. Scaling of $R(H)$ curves presented in Fig. 5.

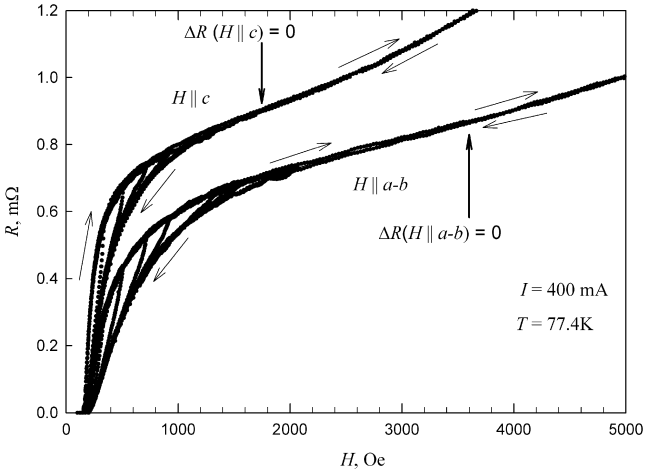

Fig. 7. Hysteretic magnetoresistance $R(H)$ of textured ceramic for $\boldsymbol{H} \parallel c$ and $\boldsymbol{H} \parallel a$–$b$ at $T = 77.4$ K. External field H was cycled up to 0.3, 0.5, 0.7, 0.9, 1.3, 1.5, and 12 kOe. Thin arrows indicate direction of scanning of external field. Bold arrows mark the field of irreversibility.

induction $\boldsymbol{B}_{\rm Jm}$ in the boundaries between Bi2223 crystallites is the vector sum of external field and field $\boldsymbol{B}_{\rm ind}$ induced by magnetic moments of neighbor Bi2223 crystallites:

$$\boldsymbol{B}_{\rm Jm} = \mu_0 \boldsymbol{H} + \boldsymbol{B}_{\rm ind}, \tag{1}$$

where μ_0 is the magnetic permeability of vacuum.

Fig. 1 shows schematically the lines of $\boldsymbol{B}_{\rm ind}$ caused by the magnetic moments of crystallites for different orientations of $\boldsymbol{H}$ and crystallographic axes of crystallites. The magnitude of $B_{\rm ind}$ is proportional to the magnetization of HTSC crystallites, $B_{\rm ind} \sim M$. It is seen that $\boldsymbol{B}_{\rm ind}$ is co-directional to the external field when field is increased ($H = H_\uparrow$). When H is decreased $B_{\rm ind}$ is also co-directional to H in the range of field where the magnetization is negative, but the magnitude $B_{\rm ind}(H_\downarrow)$ is less than $B_{\rm ind}(H_\uparrow)$ so far as $|M(H_\uparrow)| > |M(H_\downarrow)|$. In the range of $H_\downarrow \leqslant 50$ Oe the magnetization is positive, see Fig. 2a, therefore $\boldsymbol{B}_{\rm ind}$ is directed opposite to $\boldsymbol{H}$. It can result in appearance of minimum on the $R(H_\downarrow)$ dependence in the low magnetic field range [10] if transport current I larger than critical current $I_c(H_\downarrow = 0)$. This case was studied in detail for YBCO + CuO composites in Ref. [10].

The dissipation in the intercrystallite boundaries is determined by the magnetic induction $B_{\rm Jm}$ such that $R \sim B_{\rm Jm}$. Therefore, the hysteresis of magnetoresistance originates from the difference of magnitudes of $B_{\rm Jm}$ in the intercrystallite media when the external field is increased or decreased. $B_{\rm ind}(H_\uparrow)$ is larger than $B_{\rm ind}(H_\downarrow)$, therefore $R(H_\uparrow) > R(H_\downarrow)$ at $H_\uparrow = H_\downarrow$, that leads to hysteretic behavior of the $R(H)$ dependences.

3.2.2. Anisotropy of hysteresis of magnetoresistance

The anisotropy of magnetization $M(H)$ of textured sample causes the anisotropy of magnetoresistance $R(H)$ in the range $H < 2$ kOe (where the dissipation takes place mainly at the intercrystallite boundaries). Really, the module $|M_{H \parallel a-b}|$ is always less than $|M_{H \parallel c}|$, see Figs. 2–4. Therefore $\mathbf{B}_{\rm ind}^{H\parallel c} > \mathbf{B}_{\rm ind}^{H\parallel a-b}$ at $H_\uparrow = {\rm const}$ such that $B_{\rm Jm}^{H\parallel c} > B_{\rm Jm}^{H\parallel a-b}$ and $R_{H \parallel c}(H_\uparrow) > R_{H \parallel a-b}(H_\uparrow)$. In the field range above the irreversibility field the anisotropy of magnetoresistance seems to arise from intrinsic properties of crystallites.

From the other hand, the anisotropy of $\Delta M(H)$ curves (Figs. 2 and 3b) results in the anisotropic HMR measured at the same current for $\boldsymbol{H} \parallel a$–$b$ and $\boldsymbol{H} \parallel c$. So far R is proportional to $B_{\rm ind}$, therefore the height of hysteresis $\Delta R(H) = R(H_\uparrow) - R(H_\downarrow)$ (at $H_\uparrow = H_\downarrow$) is proportional to $B_{\rm ind}(H_\uparrow) - B_{\rm ind}(H_\downarrow)$, hence $\Delta R(H) \sim \Delta M(H)$. Figs. 8 and 9b show $\Delta R(H)$ dependences obtained from data of Figs. 8 and 9a correspondingly. It is seen that in the low-field range

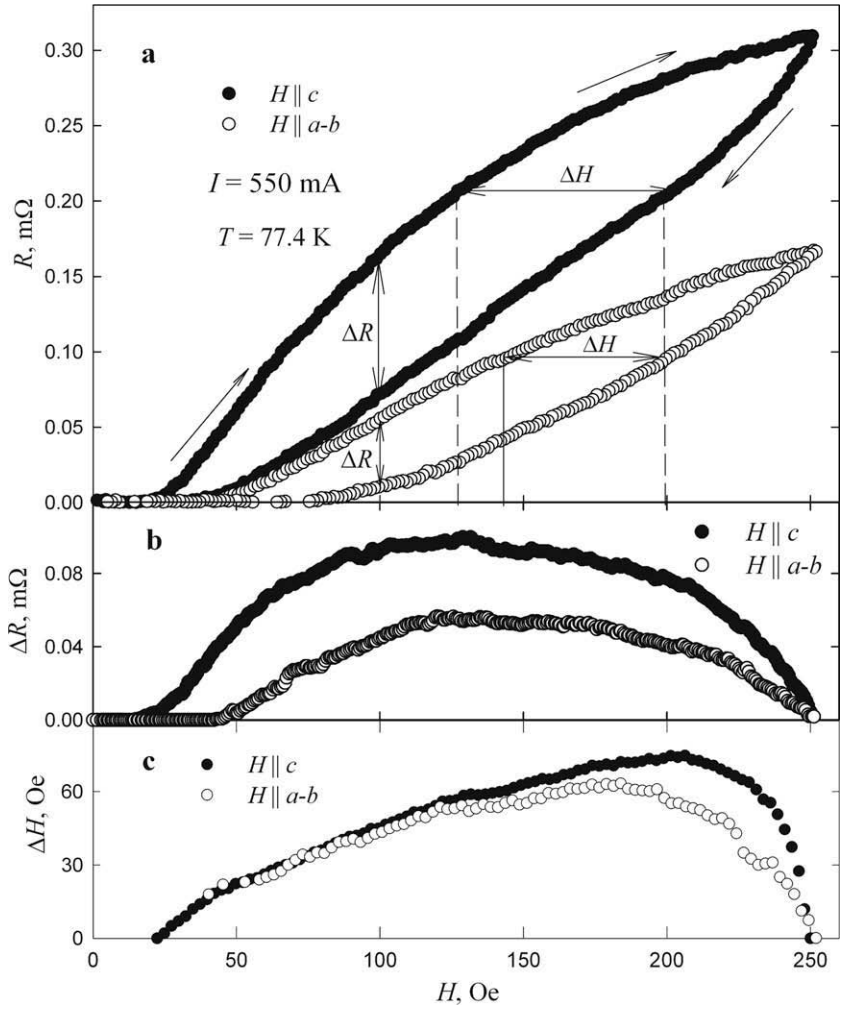

Fig. 8. Magnetoresistance of textured ceramic for $\boldsymbol{H} \parallel c$ and $\boldsymbol{H} \parallel a$–$b$ (H_{max} = 250 Oe). (a) Hysteretic magnetoresistance $R(H)$. Arrows indicate direction of scanning of external field. Double arrows show parameters characterizing hysteresis of $R(H)$: ΔH and ΔR. (b) The height of hysteresis $\Delta R(H_\uparrow) = R(H_\uparrow) - R(H_\downarrow)$ for $H_\uparrow = H_\downarrow$. (c) Magnetic width of hysteresis $\Delta H(H_\uparrow) = H_\downarrow - H_\uparrow$ for $R(H_\uparrow) = R(H_\downarrow)$.

(Fig. 8b) $\Delta R_{H \parallel c} > \Delta R_{H \parallel a-b}$. An opposite situation takes place when H is cycled up to 1600 Oe (Fig. 9b): $\Delta R_{H \parallel c} < \Delta R_{H \parallel a-b}$ in the range $H > 300$ Oe. It correlates with the behavior of $\Delta M(H)$ dependences (Figs. 2 and 3b): $\Delta M_{H \parallel c} > \Delta M_{H \parallel a-b}$ in the low-field range, while $\Delta M_{H \parallel c} < \Delta M_{H \parallel a-b}$ in the intermediate field range ($H_\uparrow \geqslant 400$ Oe).

Although $\Delta R(H) \sim \Delta M(H) \sim j_c(H)$, the resistance is a function of both B_{ind} and the transport current I. In Ref. [10] we have introduced a new parameter characterizing the hysteresis of magnetoresistance of granular HTSCs: the magnetic width of hysteresis $\Delta H = H_\downarrow - H_\uparrow$ at R = const. The main statement of [10] is that if the hysteresis of $R(H)$ is induced by the intracrystallite pinning then ΔH does not depend on the transport current I. According to above consideration (Section 3.2.1), the equality of resistance at a some values of $H_\downarrow$ and $H_\uparrow$ means the equality of total magnetic induction $\boldsymbol{B}_{Jm}$ at these fields: if $R(H_\downarrow) = R(H_\uparrow)$ for $H_\downarrow \neq H_\uparrow$ then $B_{Jm}(H_\downarrow) = B_{Jm}(H_\uparrow)$. Since (1), we obtain $H_\uparrow + B_{ind}(H_\uparrow) = H_\downarrow + B_{ind}(H_\downarrow)$ and, finally, $\Delta H = H_\downarrow - H_\uparrow = B_{ind}(H_\uparrow) - B_{ind}(H_\downarrow) \sim |M(H_\uparrow) - M(H_\downarrow)|$. Hence, the magnetic width ΔH of $R(H)$ hysteresis is determined by the magnetization of sample at points $H_\downarrow$ and $H_\uparrow$ [10,13]. An example of determination of ΔH is shown in Fig. 8a. The typical $\Delta H(H_\downarrow)$ dependences obtained by treating of experimental $R(H)$ dependences (Figs. 8 and 9a) are presented in Figs. 8 and 9c correspondingly. Similarly to $\Delta R(H)$ dependences, the $\Delta H(H_\downarrow)$ ones behave likely to the $\Delta M(H)$ dependences. Namely, $\Delta H_{H \parallel c} \geqslant \Delta H_{H \parallel a-b}$ in the range of low magnetic fields, however, $\Delta H_{H \parallel c} \leqslant \Delta H_{H \parallel a-b}$ in the range of intermediate magnetic fields.

We verified that ΔH is independent of the transport current I in the range 100–1000 mA for the textured ceramics under study. From the model [10], it follows that the hysteresis of $R(H)$ is produced by the intracrystallite pinning but not intercrystallite one.

So, the model (Section 3.2.1, Fig. 1) developed to describe the hysteretic behavior of granular HTSCs explains well the anisotropy of HMR of the textured Bi2223 ceramics.

4. Conclusions

In this paper the anisotropic behavior of magnetoresistance of bulk textured $Bi_{1.8}Pb_{0.3}Sr_{1.9}Ca_2Cu_3O_x$ + Ag ceramics has been studied. It was found that the $R(H)$ dependences exhibit the peculiarity related to the onset of dissipation within Bi2223 crystallites. The contributions to the magnetoresistance from intercrystallite boundaries and Bi2223 crystallites in various magnetic fields are distinguished. It is confirmed from both magnetic and magnetoresistive measurements that $M(H)$ and $R(H)$ dependences are hysteretic in the same magnetic field range. The anisotropy of hysteresis of magnetoresistance with respect to the orientation of $\boldsymbol{H}$ and crystallographic axis of Bi2223 crystallites was observed. The anisot-

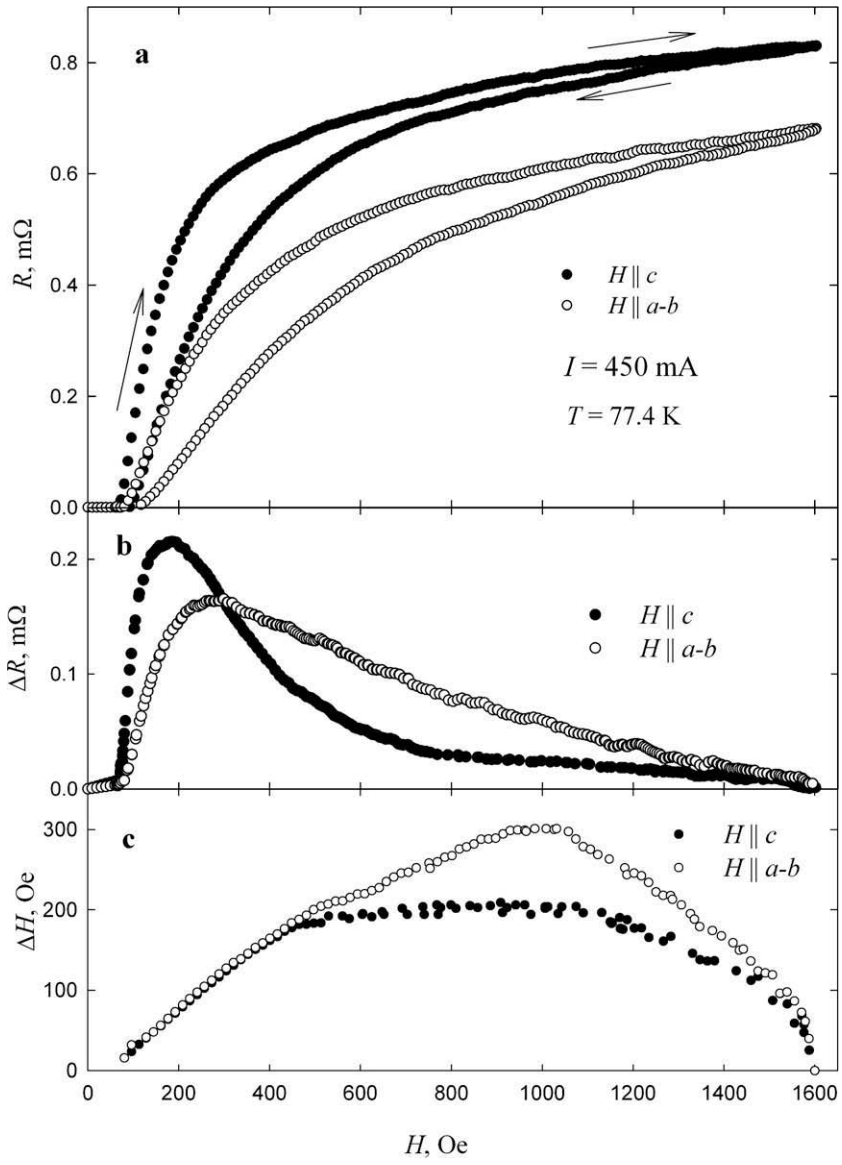

Fig. 9. Magnetoresistance of textured ceramic for $\boldsymbol{H} \parallel c$ and $\boldsymbol{H} \parallel a$–$b$ (H_{max} = 1600 Oe). (a) Hysteretic magnetoresistance $R(H)$. Arrows indicate direction of scanning of external field. (b) The height of hysteresis $\Delta R(H_\uparrow) = R(H_\uparrow) - R(H_\downarrow)$ for $H_\uparrow = H_\downarrow$. (c) Magnetic width of hysteresis $\Delta H(H_\uparrow) = H_\downarrow - H_\uparrow$ for $R(H_\uparrow) = R(H_\downarrow)$.

ropy parameter obtained by comparing the irreversibility fields of $M(H)$ (Section 3.1.1) and the analogous points of hysteretic $R(H)$ (Section 3.2.1) for $\boldsymbol{H} \parallel c$ and $\boldsymbol{H} \parallel a$–$b$ and from the scaling of $R(H)$ curves (Section 3.1.3) is ≈2.

Experimental data were analyzed within the model of granular HTSC [10], in which the intercrystallite boundaries are contained in the effective field resulting from superposition of the external field and the field induced by Bi2223 crystallites. The intercrystallite boundaries may be considered as the resistive sensor detecting this effective field. This approach allows to explain the anisotropy of hysteresis of $R(H)$ by means of the anisotropy of magnetization hysteretic loops.

Acknowledgements

Authors thanks to I.L. Belozerova for help in preparation of textured ceramics. This work was supported by program N5 of RAS, project N7, and in part in frames of young scientist projects of Siberian Federal University, project N6.

References

[1] Y.J. Quian, Z.M. Yang, K.Y. Chen, B. Zhou, J.W. Qiu, B.C. Miao, Y.M. Cai, Phys. Rev. B 39 (1989) 4701.
[2] J.E. Evetts, B.A. Glowacki, Cryogenics 28 (1988) 641.
[3] N.D. Kuz'michev, JETP Lett. 74 (2001) 262.
[4] P. Mune, E. Govea-Alcaide, R.F. Jardim, Physica C 354 (2001) 275.
[5] D. Daghero, P. Mazzetti, A. Stepanescu, P. Tura, A. Masoero, Phys. Rev. B 66 (2002) 11478.
[6] C.A.M. dos Santos, M.S. da Luz, B. Ferreira, A.J.S. Machado, Physica C 391 (2003) 345.
[7] P. Mune, F.C. Fonesca, R. Muccillo, R.F. Jardim, Physica C 390 (2003) 363.
[8] I. Felner, E. Galstyan, B. Lorenz, D. Cao, Y.S. Wang, Y.Y. Xue, C.W. Chu, Phys. Rev B 67 (2003) 134506.
[9] V.V. Derevyanko, T.V. Sukhareva, V.A. Finkel, Phys. Solid State 48 (2006) 1455.
[10] D.A. Balaev, D.M. Gokhfeld, A.A. Dubrovskii, S.I. Popkov, K.A. Shaikhutdinov, M.I. Petrov, JETP 132 (2007) 1174.
[11] V.V. Derevyanko, T.V. Sukhareva, V.A. Finkel, Tech. Phys. 53 (2008) 321.
[12] T.V. Sukhareva, V.A. Finkel, Phys. Solid State 50 (2008) 1001.
[13] D.A. Balaev, A.A. Dubrovskii, K.A. Shaikhutdinov, S.I. Popkov, D.M. Gokhfeld, Y.S. Gokhfeld, M.I. Petrov, JETP 108 (2009) 241.
[14] G.C. Han, C.K. Ong, Phys. Rev. B 56 (1997) 11299.
[15] G.C. Han, Phys. Rev. B 52 (1995) 1309.
[16] G. Grasso, R. Flukiger, Supercond. Sci. Technol. 10 (1997) 223.
[17] M. Majoros, B.A. Glowacki, A.M. Campbell, Supercond. Sci. Technol. 14 (2001) 353.

[18] B. Lehndorff, M. Hortig, H. Piel, Supercond. Sci. Technol. 11 (1998) 1261.
[19] D.C. van der Laan, J. Schwartz, Ten Haken, M. Dhalle, H.J.N. van Eck, Phys. Rev. B 77 (2008) 104514.
[20] M.I. Petrov, I.L. Belozerova, K.A. Shaikhutdinov, D.A. Balaev, A.A. Dubrovskii, S.I. Popkov, D.A. Vasil'ev, O.N. Mart'yanov, Supercond. Sci. Technol. 21 (2008) 105019.
[21] C.P. Bean, Phys. Rev. Lett. 8 (1962) 250.
[22] Li Shi, M. Fistul, J. Deak, P. Metcalf, G.F. Giuliani, M. McElfresh, D.L. Kaiser, Phys. Rev. B 52 (1995) R739.
[23] M. Pissas, D. Stamopoulos, Phys. Rev. B 64 (2001) 134510.
[24] A. Lascialfari, S. De Gennaro, A. Peruzzi, C. Sangregorio, J. Phys. D 31 (1998) 2098.
[25] P.J. Kung, M.E. McHenry, M.P. Maley, P.H. Kes, D.E. Laughlin, W.W. Mullins, Physica C 249 (1995) 53.
[26] Z. Hao, J.R. Clem, Phys. Rev. B 46 (1992) 5853.
[27] G. Blatter, V.B. Geshkenbein, A.I. Larkin, Phys. Rev. Lett. 68 (1992) 875.
[28] B. Hensel, G. Grasso, R. Flükiger, Phys. Rev. B 51 (1995) 15456.
[29] A. Oota, H. Noji, K. Ohba, Phys. Rev. B 43 (1991) 10455.